

Influence of outlet geometry on strongly swirling turbulent flow through a circular tube

M. P. Escudier,^{a)} A. K. Nickson, and R. J. Poole

Department of Engineering (Mechanical Engineering), University of Liverpool, Brownlow Street, Liverpool, Merseyside L69 3GH, United Kingdom

(Received 16 June 2006; accepted 17 October 2006; published online 12 December 2006)

The results are reported for an extensive series of measurements (using laser Doppler anemometry) of the mean and fluctuating flow fields for swirling turbulent flow downstream of an orifice in a tube. The influence of a concentric outlet contraction is found to be negligible for low “supercritical” swirl. For high “subcritical” swirl, the outlet geometry is found to have a significant influence throughout the flow field and, in the case of an eccentric (i.e., offset) outlet, to lead to an asymmetric flow with a distorted core. In no case was the core found to precess or the flow to be periodic.

© 2006 American Institute of Physics. [DOI: 10.1063/1.2400075]

I. INTRODUCTION

Swirling flows occur in a wide variety of industrial equipment, including combustion chambers, furnaces, cyclone separators, rotary kilns, turbine exhausts, and fluidic devices. By far, the most common application is to combustors, such as those used in gas-turbine engines, where high levels of swirl are introduced to the inflowing fuel and oxidant streams to improve flame stability and mixing of the reactants. Flame stability is enhanced by the recirculation, which results from the interaction between an adverse axial pressure gradient and the radial pressure variation due to swirl. Such flows are almost invariably turbulent and the mixing enhanced primarily by the rotational shear strain. The turbulence intensity (i.e., the Reynolds normal stresses) can be both amplified (especially far from the axis where the swirl-velocity distribution is free-vortex like) and attenuated (closer to the axis where the vortex structure is solid-body like) by the body forces resulting from the swirling motion. The complexity of even the isothermal-flow problem, and the difficulty of modeling it, have led to an extensive literature but the essence is described succinctly and well by Hogg and Leschziner.¹

The level (i.e., the strength or intensity) of swirl in flow through a circular tube can be described crudely in terms of the ratio of the maximum swirl velocity to the bulk axial velocity. As this ratio is increased from zero, the flow changes in character from supercritical to subcritical, roughly at the point where the velocity ratio increases above unity. In a swirling flow that is subcritical, inertial disturbances can propagate upstream from far downstream, whereas in a supercritical flow such disturbances are swept away. The criticality of swirling flows was first discussed by Squire² and the theory was further developed by Benjamin,^{3–5} who suggested that a transition region, termed “vortex breakdown,” separates conjugate supercritical and subcritical flow states. Although Benjamin’s analysis was presented in terms of relatively simple inviscid flows, subsequent work has shown that

the underlying principles apply to both laminar and turbulent vortex flows (see, e.g., Escudier⁶). Since subcritical turbulent swirling flows clearly represent a major numerical challenge, it is not surprising that there has been a significant number of papers concerned with their simulation.

The paper of Hogg and Leschziner is particularly noteworthy because it is concerned not only with the influence of swirl on turbulence, and hence the problem of turbulence modeling, but it also addresses explicitly the difficulty of handling the downstream boundary condition for a flow that remains subcritical to the outlet. In order to separate the problem of turbulence modeling from that of the downstream boundary condition, Hogg and Leschziner concluded that it was necessary to prescribe explicitly the axial-velocity distribution across the exit plane of their flow domain (i.e., a Dirichlet-type of boundary data), but accepted that this measure was unsatisfactory from a practical point of view. Other investigators who have adopted the same strategy include Chen and Lin,⁷ Yang and Ma,^{8,9} and Jakirlic *et al.*,¹⁰ while Spall and Gatski¹¹ applied a Dirichlet condition to the vorticity at outlet. Others, such as Aksel and Kaya,¹² Stein,¹³ and Kim *et al.*,¹⁴ attempted to avoid the problem by artificially extending the axial length of the flow domain sufficiently to allow the swirl to decay and the flow to return to a supercritical state. However, this approach is unsatisfactory as it is clear that extending the flow domain in this way must change the flow conditions at the actual outlet location. In some instances (examples include Darmofal,¹⁵ Xia *et al.*,¹⁶ Young *et al.*,¹⁷ Yaras and Grosvenor,¹⁸ and Herrada and Fernandez-Feria¹⁹), no mention is made of the nature of the outlet flow, and standard boundary conditions typical of non-swirling flows (e.g., Neumann type of boundary data) are applied without comment on their appropriateness.

It has long been recognized that experimental observations are crucial for the validation of turbulence models and to test their application to particular problems. For the reasons already discussed, this need is even greater for subcritical turbulent swirling flows. Several experimental studies have been reported for turbulent swirling flows that exhibit subcritical flow characteristics throughout the entire region downstream of the recirculation zone in combustor-type ge-

^{a)}Author to whom correspondence should be addressed. Electronic mail: escudier@liv.ac.uk

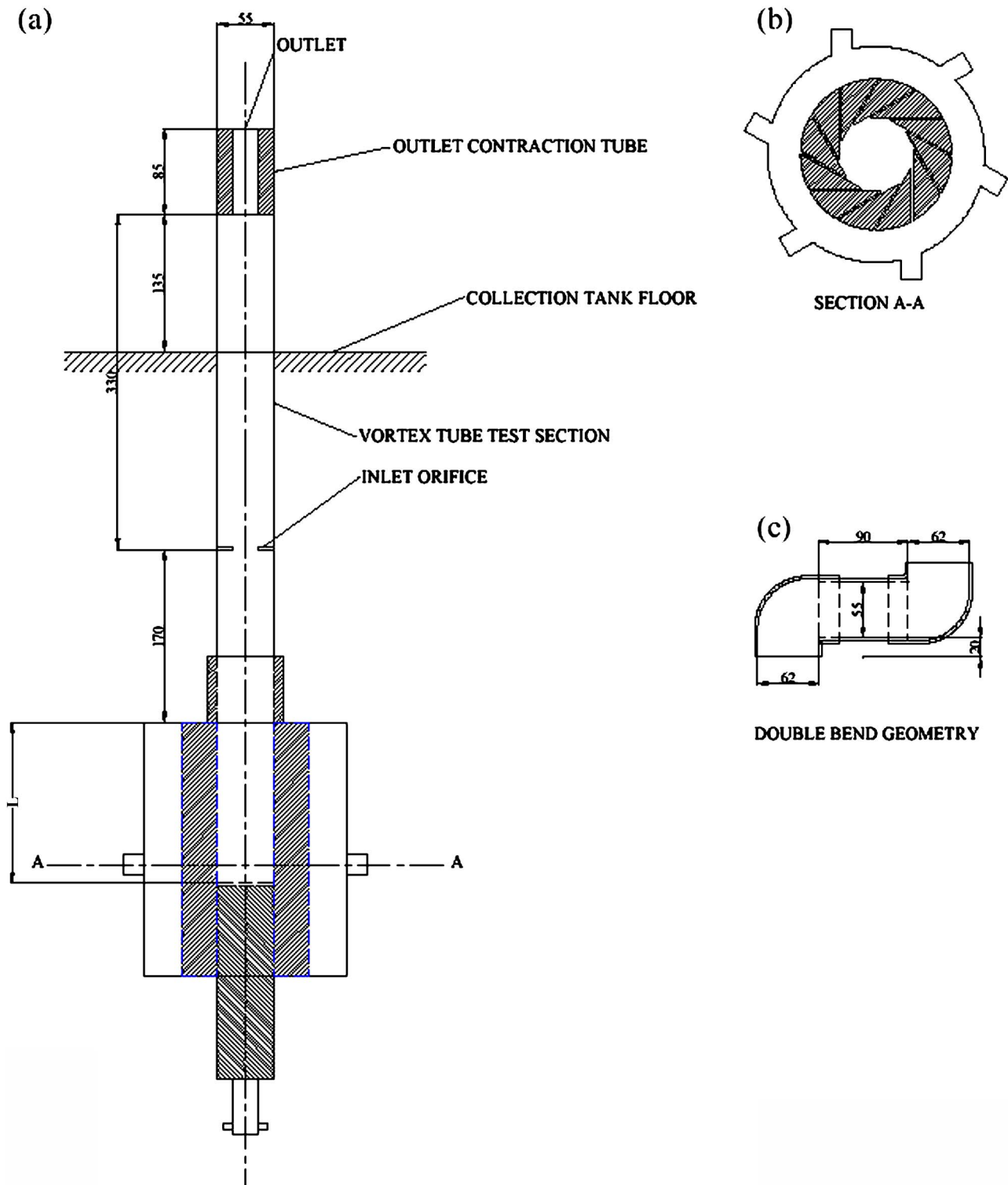


FIG. 1. Basic layout of swirl generator and pipe assembly with details of the swirl generator and the double-elbow outlet (all dimensions in mm).

ometries. Early papers dealing with such flows include those of Altgeld *et al.*,²⁰ So *et al.*,²¹ and Escudier and Keller,²² with more recent work by Ahmed and Nejad,²³ Doebbeling *et al.*,²⁴ Khezzar,²⁵ Huang and Tsai,^{26–28} Schmitt *et al.*,²⁹ Huang and Yen,³⁰ and Al-Abdeli and Masri.³¹ Escudier and Keller discussed the problem of the downstream boundary condition for a subcritical flow and reported on the influence on the upstream flow of three concentric outlet contractions

(plus the fully open case) whereas all other papers are limited to one outlet condition in each case. The study of Escudier and Keller did not include turbulence data but was restricted to measurements of the mean flow. Some of the other studies mentioned above have included turbulence measurements, but what has been lacking hitherto has been a systematic experimental study of the influence of a wider range of outlet geometries on a swirling turbulent flow that remains subcriti-

TABLE I. Flow parameters for LDA measurements.

Outlet geometry		\dot{Q} (m ³ /s)	Re_E	Re	L (mm)	Ω	S_E	S
(a)	Fully open	6.71×10^{-5}	3440	1565	95	2.98	0.30	0.12
	55 mm ϕ	6.52×10^{-5}	3350	1520	35	8.07	0.60	0.22
(b)	Contraction	6.71×10^{-5}	3440	1565	95	2.98	0.34	0.14
	25 mm ϕ , 85 mm long	6.52×10^{-5}	3350	1520	35	8.07	0.61	0.21
(c)	Eccentric contraction	6.52×10^{-5}	3350	1520	35	8.07	0.66	0.25
	25 mm ϕ , 85 mm long 13.2 mm offset							
(d)	Concentric annular disk 49 mm ϕ	6.52×10^{-5}	3350	1520	35	8.07	0.64	0.25
(e)	Double 90° elbow 55 mm ϕ [see Fig. 1(c)]	6.52×10^{-5}	3350	1520	35	8.07	0.58	0.21

cal downstream of vortex breakdown. Such a study is needed to provide a benchmark data set for researchers developing techniques to model or apply such numerical methods as large eddy simulation and direct numerical simulation to complex turbulent flows. In the present paper we discuss the results of measurements for five different outlet geometries: fully open, a concentric central contraction, a concentric annular contraction, an eccentric contraction, and a fully open double elbow. For each of the contraction geometries, the area reduction was just below 80%, the same as that for one of Escudier and Keller's outlets although their upstream geometry was quite different from that adopted here. For comparison, we also present data for two flows that have returned to supercritical at the outlet.

II. EXPERIMENTAL ARRANGEMENT AND INSTRUMENTATION

The experiments discussed here were carried out in a new water-flow facility not previously reported on. The overall arrangement is shown in Fig. 1, which includes the experimental arrangement with a concentric outlet contraction installed [Fig. 1(a)], details of the swirl generator [Fig. 1(b)] and the double-bend outlet [Fig. 1(c)]. The swirl generator is based on the tangential-inlet (slit-tube) design used by Escudier *et al.*³² but with the single-wide-inlet slit used in their arrangement replaced by 12 narrow slits at 30° intervals with the intention of reducing the flow asymmetry observed with the single-slit arrangement. As can be seen from Fig. 1(b), the slits are created using 12 identical wedges assembled around a vertical axis. The wedges are machined from stainless steel and the width t of each slit is 1 mm. The outer diameter of the wedge assembly is 165 mm while the central channel created by the wedges is a dodecahedron with distance between opposing flat surfaces 55 mm. The open axial length L of the slits can be varied between 27 and 263 mm by adjusting the axial position of a close-fitting central piston, the cross section of which is also a dodecahedron. The swirl generator is surrounded by a cylindrical jacket of inner diameter 305 mm into which water is fed through six equally spaced 31-mm-diam inlet ports each angled to be tangential to the periphery of the wedge assembly and located halfway along its length. The water supply is fed under gravity from

a large (ca. 99 000-liter) tank some 36 m above the vortex generator, with the flowrate controlled by two needle valves arranged in parallel.

Visual observations and laser Doppler anemometer (LDA) measurements were made in a circular perspex pipe (the vortex tube) located vertically above the outlet from the vortex generator. The internal diameter of the vortex tube D is 55 mm and its full length 585 mm. To reduce refraction of the laser beams, the vortex tube was surrounded by a square optical box filled with water. Dye can be injected into the flow through a hole running along the centerline of the piston and terminating in a hole of 1 mm diam. The vortex tube discharges into a large collection tank within which the water level is below that of the tube outlet so that the outlet condition is that of a free surface.

As explained below, to achieve a large, stable vortex-breakdown structure at a convenient (for LDA measurements) location, an orifice plate was installed within the vortex tube 175 mm above the generator outlet. The five outlet geometries were as follows: (a) straight and fully open; (b) concentric circular tube of diameter 25 mm and length 85 mm, hereafter referred to as the concentric contraction; (c) circular tube of diameter 25 mm and length 85 mm eccentric to the vortex tube by a radial offset $e = 13.2$ mm ($e/D=0.24$), referred to as the eccentric contraction; (d) outlet produced by a concentric disk of diameter 49 mm (annular gap 3 mm) and referred to as the annular contraction; (e) outlet constructed from two standard 90° elbows, as shown in Fig. 1(c), mounted at the end of the vortex tube. In all three contraction cases, the area reduction is 79.3% and each one was installed in the vortex tube with its inlet 330 mm (i.e., six vortex-tube diameters) from the inlet orifice. For outlet geometry (e) the distance between the inlet orifice and the outlet was eight vortex-tube diameters (440 mm).

Measurements of the swirl (v) and axial (u) components of velocity were made within the vortex tube in forward scatter using a two-component Dantec Fibreflow LDA system comprising a 60X10 probe and 57X08 receiving optics. The beam separation at the front lens was 51.5 mm and the lens focal length 160 mm, which produced a measuring volume 280 μ m in length and 45 μ m in diameter. The LDA signals were processed using a Dantec 58N10 particle dy-

namics analyzer. Ensemble averages were formed from not less than 10 000 samples. The outlet contraction and vortex tube were marked to create a zero reference location, designated 0° , for the LDA measurements. For outlet geometries (c) and (d), for which it was necessary to perform LDA measurements at a number of different azimuthal orientations [see Sec. V], the outlet was rotated relative to the fixed position of the LDA system. The flowrate was measured using an Endress & Hauser Promass 60 Coriolis mass flowmeter.

III. FLOW PARAMETERS

If the volumetric flowrate is \dot{Q} and the vortex-tube diameter is D , then the bulk axial-flow velocity in the vortex tube is $U=4\dot{Q}/\pi D^2$. If there are n slits (here $n=12$) each of width t (1 mm), then the average tangential flow velocity V at exit from a slit with open length L is \dot{Q}/ntL . A crude estimate for the circulation is then $\Gamma=\pi VD=\pi\dot{Q}D/ntL$ and, as suggested by Escudier *et al.*,³³ a simple geometric measure of the swirl strength Ω is given by

$$\Omega = \Gamma/UD = \pi^2 D^2/4ntL. \quad (1)$$

A more conventional measure of swirl intensity is obtained from the axial and angular momentum flowrates. At the outlet plane of the inlet orifice the swirl strength S_E is given by

$$S_E = 2A_E/M_E D_E, \quad (2)$$

where

$$A_E = 2\pi\rho \int_0^{R_E} uvr^2 dr \quad (3)$$

is the flowrate of angular momentum through the inlet orifice and

$$M_E = 2\pi\rho \int_0^{R_E} u^2 r dr \quad (4)$$

is the corresponding flowrate of axial momentum.

Similar expressions to the above can be written down for the flow in the vortex tube itself in terms of A , M , and D from which an alternative swirl parameter S can be calculated. A and M are defined in the same way as A_E and M_E with the upper limit R_E in the integrals replaced by R . The Reynolds numbers corresponding to S and S_E are $Re = UD/\nu$ and $Re_E = U_E D_E/\nu$, where $U_E = 4\dot{Q}/\pi D_E^2$ is the bulk velocity for flow through the inlet orifice.

The series of flow-visualization tests reported below, used to determine the conditions for detailed flow measurements using LDA, were characterized in terms of the geometric parameter Ω and the Reynolds numbers Re and Re_E , whereas for the LDA measurements the swirl parameters S_E and S were also evaluated and are listed in Table I. The kinematic viscosity ν of water was taken as $0.993 \times 10^{-6} \text{ m}^2/\text{s}$ (corresponding to the average water temperature of 20.4°C).

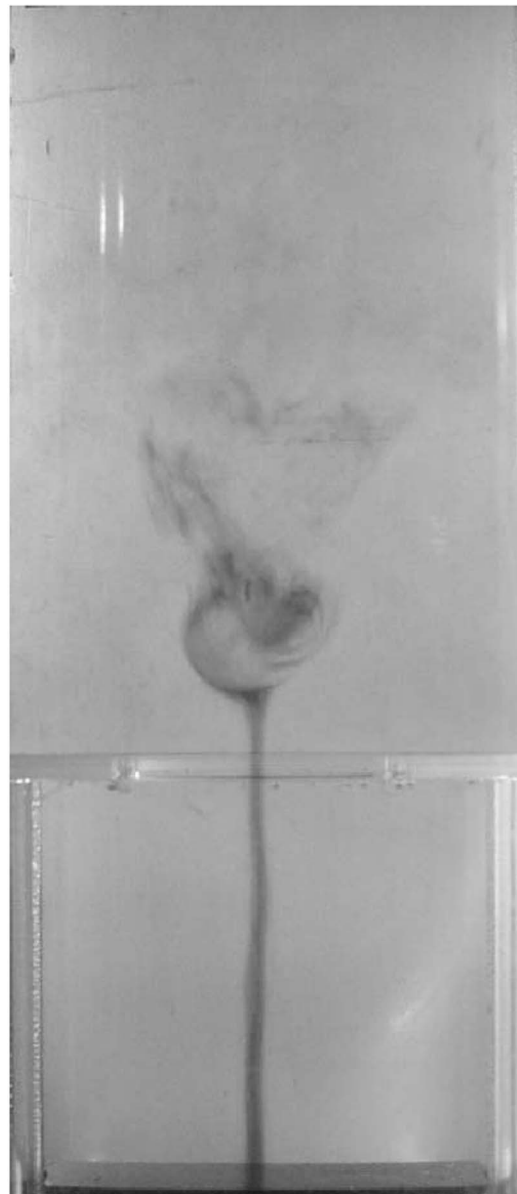


FIG. 2. Visualization of low-swirl vortex breakdown for $Re_B=1565$, $\Omega_B=2.98$, and $D_E=25$ mm.

IV. FLOW VISUALIZATION SCOPING EXPERIMENTS

To establish the most suitable swirl and flowrate settings for the LDA measurements, a series of preliminary flow-visualization experiments was carried out. Observations using a blue dye (“Berlin blue” food coloring) were made for a range of values of the geometric swirl parameter Ω of the flow downstream of each of a series of concentric orifice plates installed in the vortex tube 175 mm downstream of the swirl generator. Seven different orifice plates were used with diameters D_E in the range 12.5–35 mm with the value of Ω set by varying the open length L of the generator slits. The flowrate was adjusted until a region of recirculation (vortex breakdown) was observed on the vortex-tube axis approximately 10 mm downstream of the orifice plate. A typical low-swirl flow-visualization example is shown in Fig. 2.

The results plotted in Fig. 3 reveal fairly well-defined relationships between the breakdown Reynolds number Re_B

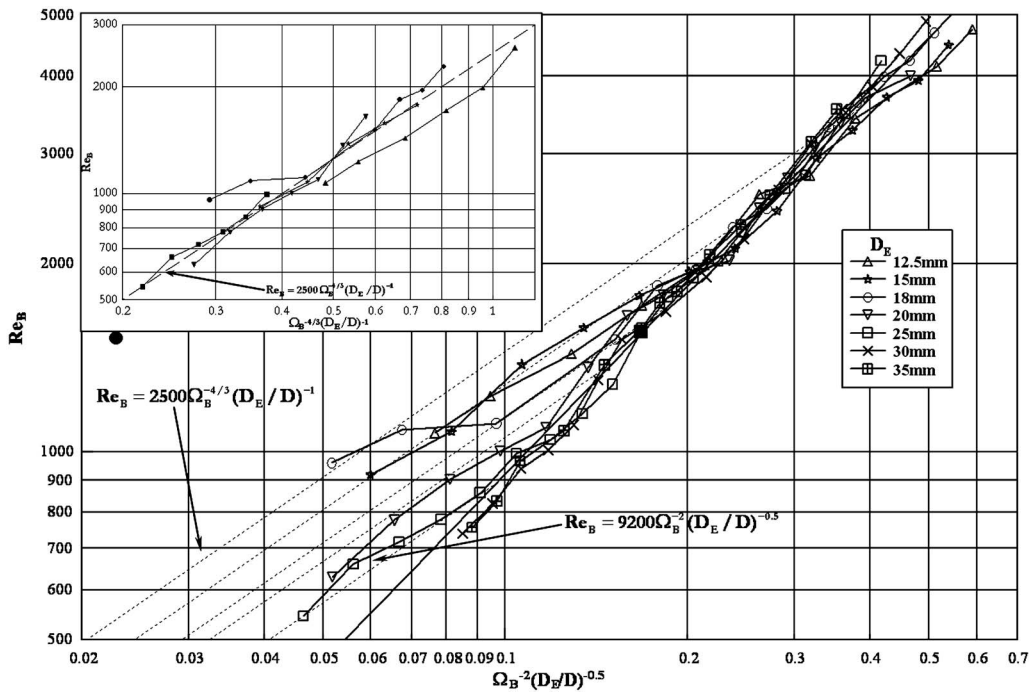


FIG. 3. Dependence of Reynolds number Re_B for vortex breakdown on geometric swirl number Ω_B and orifice:pipe diameter ratio D_E/D . LDA measurements were carried out for parameter combinations corresponding to the symbols (●) and (■).

($=U_B D/\nu$, where U_B is the bulk velocity in the vortex tube corresponding to a breakdown), the swirl parameter for breakdown Ω_B , and the diameter ratio D_E/D . For each diameter ratio, the data asymptote towards

$$Re_B \Omega_B^2 \sqrt{D_E/D} = 9200 \quad (5)$$

for the higher Reynolds numbers, whereas at lower Re_B values the limited data available (also shown in the inset of Fig. 3) correlate roughly with

$$Re_B \Omega_B^{4/3} D_E/D = 2500. \quad (6)$$

The values of Re_B , where the two correlations intersect, are easily calculated as 3574 (for $D_E=12.5$ mm), 2482 (15 mm), 1724 (18 mm), 1396 (20 mm), 893 (25 mm), 620 (30 mm), and 456 (35 mm), and the terms higher and lower here refer to values above and below the intersection values. For vortex breakdown in tubes downstream of the slit-tube vortex generator of Escudier *et al.*,³² Escudier³³ gave the criterion for breakdown as

$$\Gamma^2/(\nu L U_E) = \text{const}, \quad (7)$$

which, for the present situation in which n , t , and D are fixed, can be shown to be equivalent to

$$Re_B \Omega_B^3 (D_E/D)^3 = \text{const}. \quad (8)$$

Equation (7) was derived assuming $D_E/L \ll 1$ which, in general, is not the case here. Although Eq. (8) indicates a stronger dependence of Re_B on both Ω and D_E , it is qualitatively consistent with Eqs. (5) and (6) in the sense that it confirms the experimental observation that increasing either the level of swirl or the orifice diameter will reduce the Reynolds number at which vortex breakdown can be expected to occur.

It should be noted that some of the breakdowns observed were better defined than others and that in no case was the breakdown completely stationary but tended to move, both axially and radially, around a mean position in an apparently random (i.e., nonperiodic) manner. The limitation to Re values below about 5000 was set by the onset of gaseous cavitation of the vortex core.

V. DISCUSSION OF LDA MEASUREMENTS OF MEAN FLOW

For the low-swirl measurements discussed below, the parameter combination chosen was $Re_B=1565$, $\Omega_B=2.98$ (with $L=95$ mm), and $D_E=25$ mm (i.e., $D/D_E=2.2$), which corresponds with the closed square symbol (■) in Fig. 3, as this produced a relatively large, well-defined breakdown and (as the LDA measurements confirm) a flow that became supercritical far downstream. The high-swirl measurements, which constitute the bulk of the measurements presented in this paper, were produced by the combination $Re_B=1520$, $D_E=25$ mm, and $\Omega_B=8.07$ ($L=35$ mm), for which the flows remained subcritical far downstream corresponding to the closed circle symbol (●) in Fig. 3. In the absence of swirl, the observations of Pak *et al.*³⁴ for flow through two axisymmetric sudden expansions with D/D_E values of 2.0 and 2.7 (i.e., similar to those in the current study) showed that for Re_E less than about 800, the downstream flow was laminar, whereas for Re_E greater than about 2000, it was turbulent. However, it is well known (see, e.g., Herrada *et al.*³⁵) that even a small amount of swirl significantly modifies flow in a pipe, and the critical Reynolds numbers for transition of swirling flows are much lower than those for nonswirling flows. The combinations of Reynolds number and swirl lev-

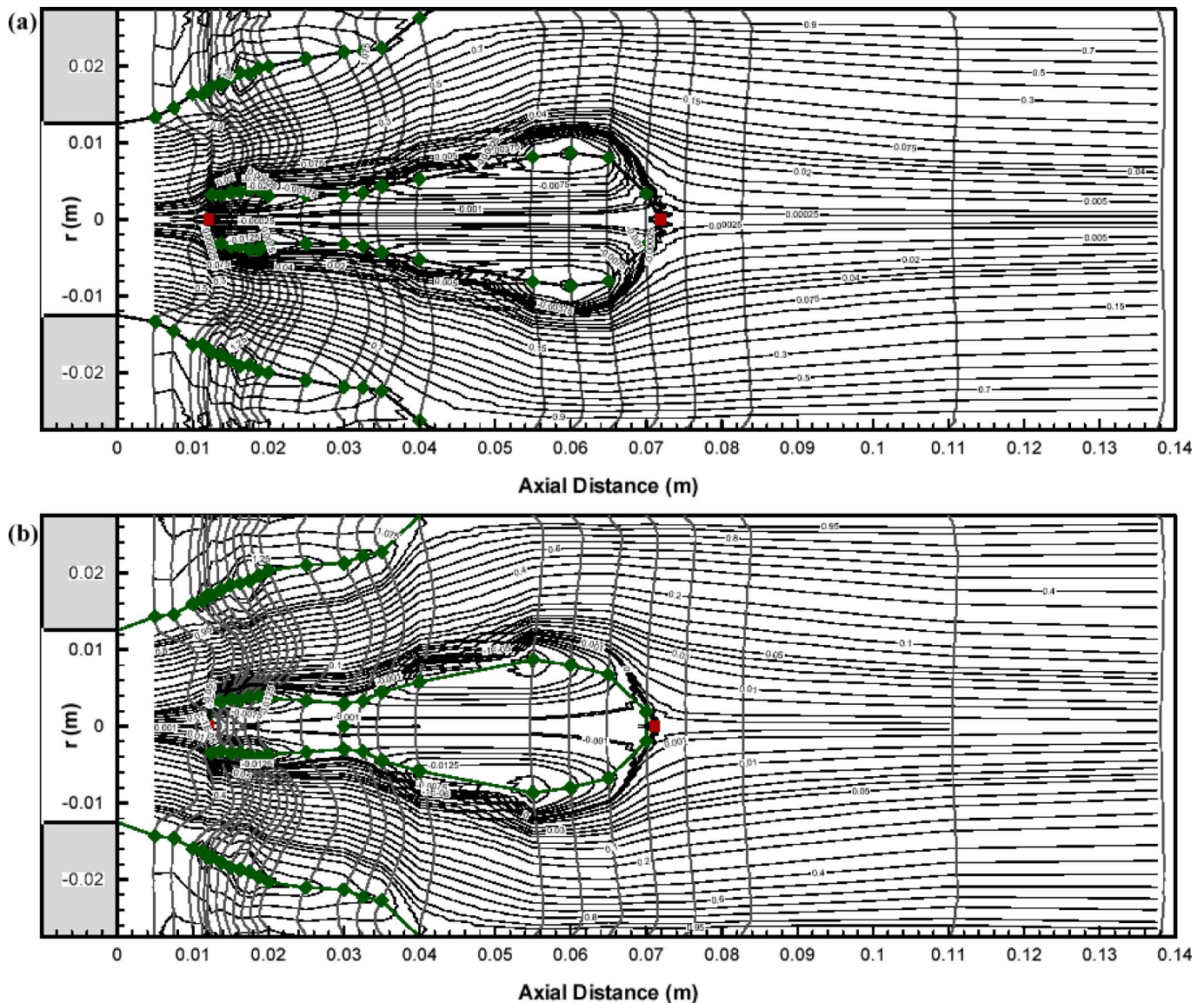


FIG. 4. Streamline patterns with axial-velocity profiles superimposed (a) $S=0.3$, fully open outlet; (b) $S=0.34$, 25 mm ϕ outlet contraction. (\blacklozenge) denotes zero axial velocity, (\blacksquare) a stagnation point, and (—) $\psi=0$.

els in all the measurements presented here lead to flows with very high turbulence levels and are consistent with the foregoing statements.

For each parameter combination, initial measurements were made of the radial distributions of the swirl (i.e., tangential) velocity $v(r)$ at a series of axial locations x [see Fig. 1(a)], measured from the inlet orifice, to establish whether the vortex core was axisymmetric. The closest location to the inlet orifice that could be reached with the LDA system before the laser beams (oriented for measurement of the axial-velocity component u) were impeded by the swirl generator was $x=5$ mm. The furthest x location that could be reached downstream, due to the position of the collection tank, was about 140 mm. The selection of intermediate locations was guided by the measurements themselves to provide sufficient detail, e.g., to establish the internal structure of the vortex-breakdown region. If the $v(r)$ profiles revealed appreciable departures (more than 0.5 mm) of the vortex core axis from

axisymmetry, additional measurements were made to establish the angular θ_C /radial r_C location of the core axis at each axial location using the procedure to determine r_C and θ_C described in the Appendix. The measurements of the $v(r)$ profiles were then repeated with the LDA system oriented to ensure the radial path of the measuring volume passed through the offset vortex axis. Axial-velocity profiles $u(r)$ were then measured at the same axial locations as the $v(r)$ profiles, again ensuring appropriate orientation of the LDA system. Where flows were found to be axisymmetric, axial-velocity distributions $u(r)$ were measured at additional x locations to assist in constructing streamline patterns.

It is inherent in the LDA technique that the instantaneous velocity measurements can be analyzed to obtain both temporal average and rms values as well as frequency spectra. However, it is well known that there are difficulties in estimating spectra due to the discrete nature of the LDA bursts. In the study reported here we used a sample and hold meth-

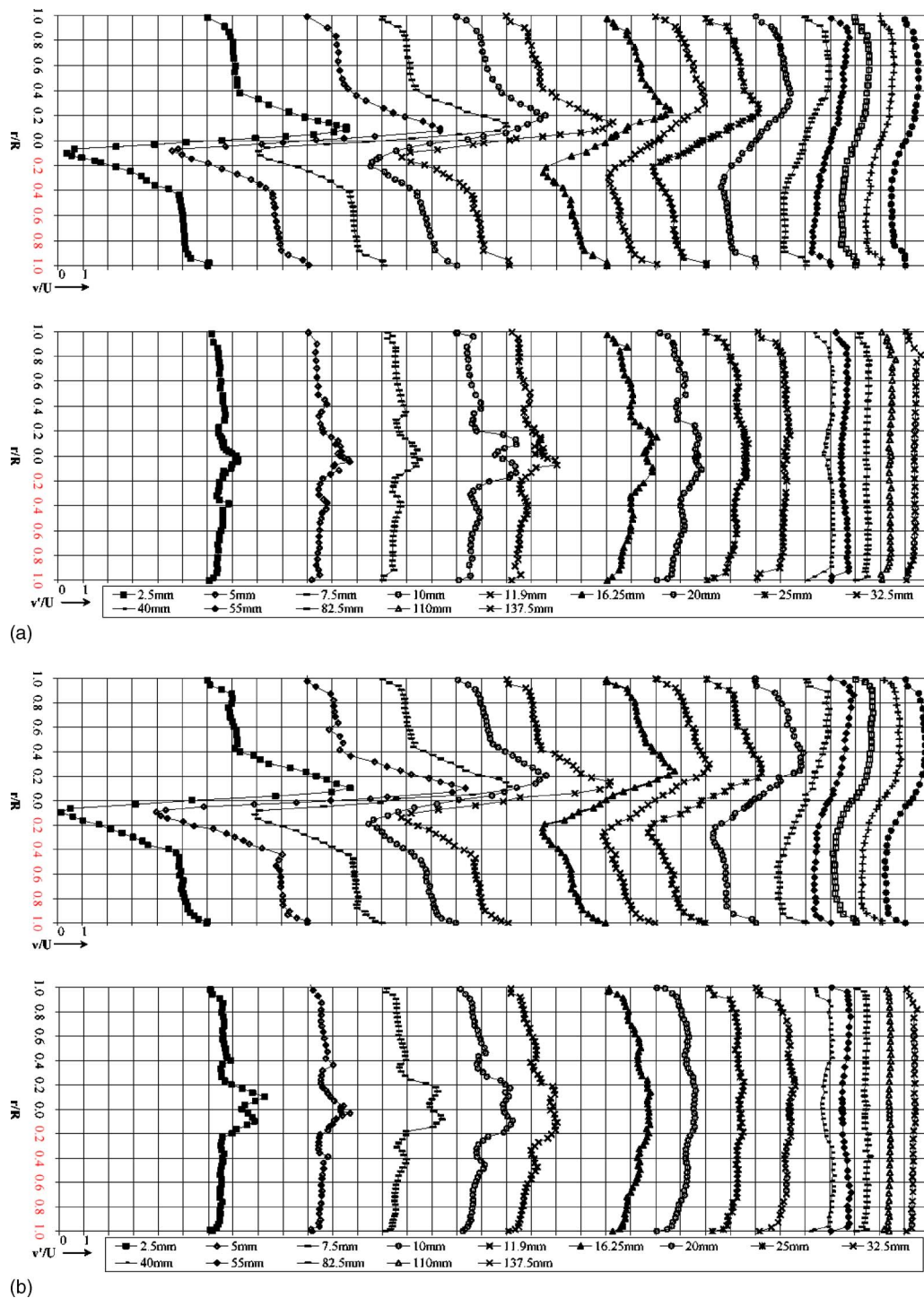


FIG. 5. (a) Radial distributions of mean swirl velocity and swirl-velocity fluctuations at all x locations from for low swirl, $S_E=0.3$, fully open outlet. (b) Radial distributions of mean swirl velocity and swirl-velocity fluctuations at all x locations for low swirl, $S_E=0.34$, 25 mm ϕ concentric outlet contraction.

odology to produce a continuous time history of the velocity signal, and then obtained spectra using a fast Fourier transform (FFT). At each (x, r, θ) location, a minimum of 10 000 valid samples was acquired by the LDA system from which to evaluate an ensemble average for these quantities. It is well known (see, e.g., Gupta *et al.*³⁶) that swirl-flow geometries can lead to the phenomenon of the precessing vortex core (PVC), i.e., the vortex core precesses around the tube axis at a frequency which can be detected from frequency

spectra. As remarked earlier, from our visual observations it appeared that the vortex breakdown itself moved randomly rather than periodically, i.e., none of our vortex flows exhibited precession of the vortex core. This observation was confirmed by the absence of well-defined peaks in the spectra obtained from our LDA measurements. The profiles of rms values, u' and v' , which we present here, are thus Reynolds normal stresses (turbulence intensities) “uncontaminated” by the effects of precession. Although the radial distributions of

u' and v' are included in the same figures as the profiles of the mean velocity components, u and v , they are discussed separately in Sec. VI.

For flows showing negligible departure from axisymmetry, streamline maps were constructed from values of the stream function $\psi = 2\pi \int_0^r u r dr$ calculated from the mean axial-velocity distributions. For the calculation of ψ , values of u at the same r location on either side of the axis were averaged. The values of ψ were then normalized with the value for each x location at $r=R$ (i.e., essentially the volumetric flowrate).

A. Low-swirl, $S_E \approx 0.3$, fully open and central concentric contraction

For each of the two low-swirl situations, the streamline patterns are shown in Fig. 4. Superimposed on each of the streamline maps are the corresponding axial-velocity profiles. The values on each streamline correspond to the normalized ψ value. The streamline maps reveal two closed areas of recirculation. There is an elongated recirculation bubble centered on the pipe axis and starting slightly downstream of the orifice, indicative of vortex breakdown. The outer toroidal region of recirculation immediately downstream of the orifice is a consequence of the sudden area expansion and has a reattachment length of about 40 mm or slightly less than three step heights. The flow is essentially unaffected by the outlet geometry which is fully open for Fig. 4(a) and includes a concentric tube 25 mm in diameter (i.e., 79% area reduction) and 85 mm long, located 330 mm from the inlet orifice for Fig. 4(b). We interpret the insensitivity of the flow to the outlet condition as indicating that the swirl intensity downstream of vortex breakdown decays and the flow quite rapidly becomes supercritical, i.e., the propagation speed of longitudinal inertia waves for this flow is lower than the average axial-flow speed. A more precise determination of whether an experimental flow is supercritical or subcritical, e.g., using Benjamin's³ critical equation, is practically impossible.

Swirl profiles $v(r)$ for the fully open outlet are shown in Fig. 5(a). For clarity, the spacing of the profiles has been chosen to minimize overlap and does not therefore represent the true physical spacing. Several key features of the flow are apparent: the swirl profiles have a structure comprising an inner core of solid-body rotation within which the swirl velocity progressively decays with downstream distance; an outer region extending to about $0.9R$, where the flow is probably influenced by large-scale Görtler vortices; and a near-wall boundary layer. Superposition of the swirl profiles (not shown here) reveals that there is a region extending to about $0.4R$ within which all profiles are bounded by an envelope curve. A similar four-region structure for a swirling flow has been identified in a very recent paper by Zhang and Hugo.³⁷ The peak swirl velocity in the vortex core decays from about $5.5U$ at exit from the inlet orifice to about $0.5U$ one diameter downstream and beyond. As the swirl decays, the core radius (measured as the radial distance to the swirl-velocity peak) increases progressively from about 0.1 to $0.6R$. Further de-

cay of the swirl profile beyond one diameter downstream of the inlet orifice is imperceptible.

From Fig. 5(b) for the 25-mm ϕ concentric outlet contraction, it is clear that for the low-swirl case the exit condition has only a minor influence on the flow field and the differences compared with the fully open outlet are slight. Close to the inlet orifice ($x=2.5$ to 7.5 mm) the vortex core is slightly broader than for the fully open case, and the peak velocity at $x=5$ mm is slightly higher. A higher peak velocity is also seen at $x=32.5$ mm. Further downstream ($x > 82.5$ mm), the swirl velocities are seen to be higher across the entire cross section for the contraction case than for the equivalent profiles for the fully open case (e.g., for $x = 137.5$ mm at $r/R=0.4$ the difference in the velocity between the two cases is 30%) with a slight asymmetry also noticeable.

The corresponding variation of the axial-velocity component shown in Fig. 6(a) is clearly far more complex. Here again the spacing of the profiles has been selected to minimize overlap and is different from the distribution used in the swirl-velocity figures. Figure 6(a) shows that between the inlet orifice and $x=10$ mm ($x/D=0.18$) the axial-velocity is jet like within the vortex core with a peak velocity on the centerline of about $9U$, though this decays rapidly to a wake-like form further downstream becoming negative at about $x = 12$ mm ($x/D=0.22$). The maximum reverse-flow velocity, on the axis at about $x=17.5$ mm, is seen to be about $-2U$. The recirculation evident in the streamline plots corresponds to the combination of these negative core velocities and the positive axial velocities surrounding the core where the peak velocity reaches $5.5U$. The progressive change to forward flow over most of the tube cross section downstream of the recirculation bubble is apparent, though the wake-like deficit on the centerline is still evident at the last measuring location but clearly diminishing. The centerline velocity here is still 25% lower than the peak velocity (at about $r/R=0.8$). Comparison with the axial-velocity component for the 25-mm ϕ concentric outlet contraction, Fig. 6(b), confirms that the addition of an exit contraction has no significant effect on the flow for this swirl number and Reynolds number combination.

B. High-swirl $S_E \approx 0.6$, fully open and concentric contraction

In contrast to the low-swirl supercritical-flow case, the streamline patterns for the high-swirl situation are entirely different for the two exit conditions which we take to indicate that the downstream flows remain subcritical. For the fully open case, Fig. 7(a), there is reverse flow along the vortex core all the way to the inlet orifice and, in fact, even penetrating into the region upstream of the orifice plate: the (\blacklozenge) symbols denote the locations of zero axial velocity. The outer toroidal region of recirculation is considerably shorter than for the low-swirl situation (reattachment length about 25 mm or $x/D=0.45$ compared with 40 mm or $x/D=0.82$). The shorter reattachment length is associated with a bulge in the streamline patterns within one diameter of the orifice. The bulge does not close as in the supercritical case to form

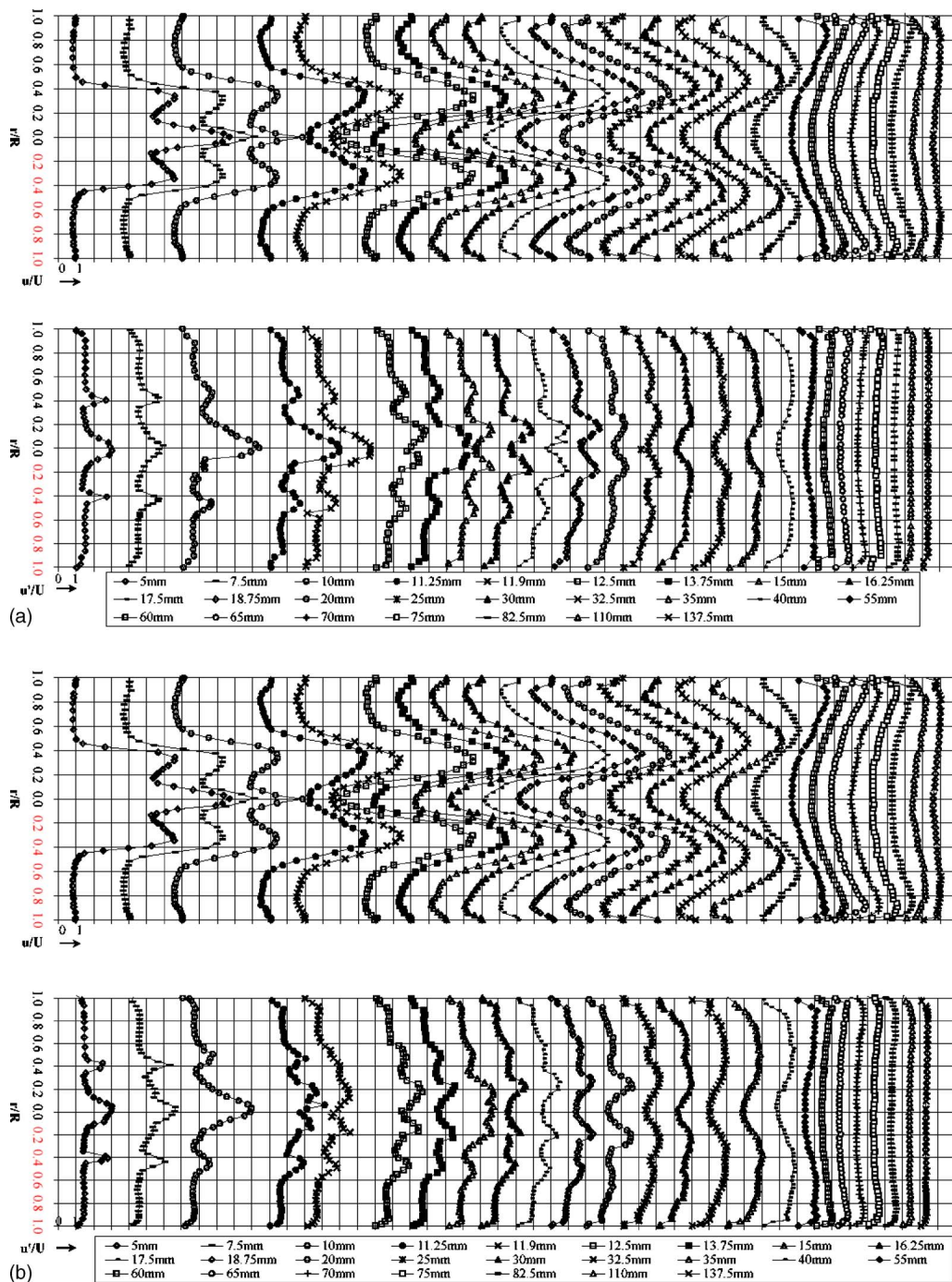


FIG. 6. (a) Radial distributions of mean axial velocity and axial-velocity fluctuations at x locations, $S_E=0.3$, fully open outlet. (b) Radial distributions of mean axial velocity and axial-velocity fluctuations, $S_E=0.34$, 25 mm ϕ concentric outlet contraction.

a recirculation “bubble”; instead, the streamlines initially converge downstream (in the region $25 \text{ mm} < x < 55 \text{ mm}$) and then stay more or less cylindrical throughout the measurement region.

With the 25-mm-diam concentric outlet contraction installed, the streamline patterns shown in Fig. 7(b) reveal a compact central region of recirculation in the near vicinity ($x < D$) of the inlet orifice and a jet-like flow further downstream (beyond about one diameter from the inlet orifice). This recirculation zone exhibits some of the characteristics of vortex breakdown, such as recirculation with reverse flow

along the axis, but is clearly far more complex in structure than the well-defined bubbles shown in Fig. 4. The outer recirculation zone is again shorter (ca. 27 mm or $x/D=0.49$) than for the low-swirl case. The streamlines in Fig. 7(b) are qualitatively representative of the flow structure but the strong “unphysical” distortions near $x=25$ and 50 mm are probably the consequence of asymmetries in the velocity profiles (see below) that develop in this region, where velocity gradients are steep and the flow structure is changing rapidly with downstream location.

As with the figures for low swirl, the data shown in Fig.

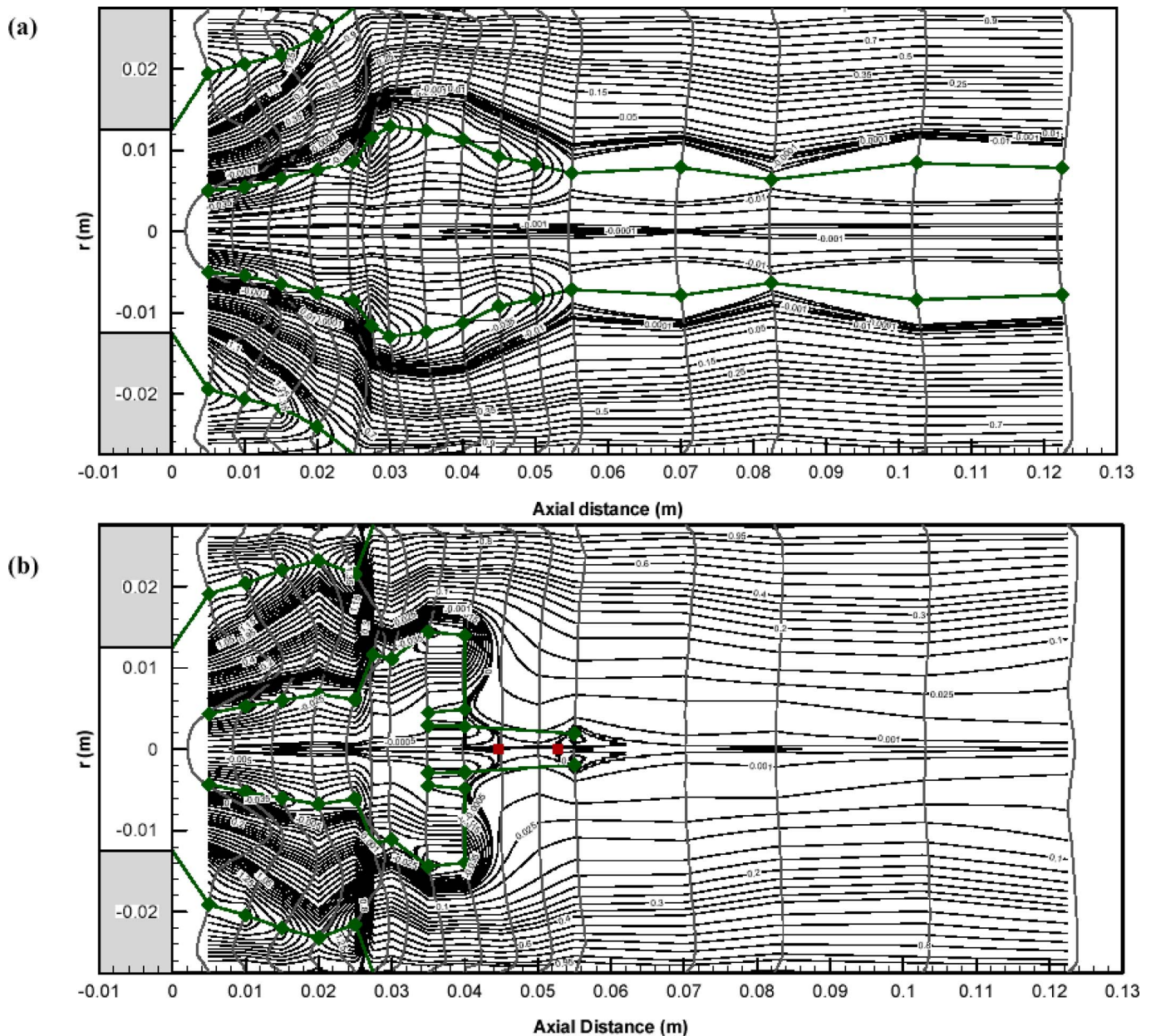


FIG. 7. Streamline patterns constructed from axial-velocity distributions with axial-velocity profiles superimposed: (a) $S_E=0.6$, fully open outlet; (b) $S_E=0.61$, 25 mm ϕ outlet contraction. (\blacklozenge) denotes zero axial velocity; (\blacksquare) a stagnation point, and ($-$) $\psi=0$.

8 have been plotted to minimize overlap between the profiles, which is not representative of the true physical separation of the axial locations. Even at the first measuring location ($x=5$ mm), the swirl profiles reveal an important qualitative difference: for the contraction case [Fig. 8(b)] the core profile is practically linear (solid-body rotation) much as for the low-swirl flows, whereas the fully open case exhibits a central inflection within a narrow region close to the centerline ($r/R \approx 0.1$). For both of these profiles the peak tangential velocity is close to $8U$ and both have a quadruple structure: a slender inner core ($r < 0.3R$) with very steep gradients; a region surrounding the core out to $r/R=0.6$, again with very steep gradients where v falls by 50%; a region out to $0.9R$ where the swirl has a free-vortex ($v \sim 1/r$) form; and a final “boundary-layer” region. By the second measuring location ($x=10$ mm), the free-vortex region has disappeared

and the boundary layer has grown to a thickness of $0.4R$, the core has broadened to a diameter $\phi \approx 0.8R$, and the peak tangential velocity has dropped to about $5U$. In both cases solid-body rotation is limited to about $r \approx 0.06R$ with the gradient for the contraction geometry about three times that for the fully open outlet. Beyond $x=15$ mm, the most significant qualitative difference is the appearance of a double-peak structure with the contraction: there is an inner core ($\phi \approx 0.2R$) of solid-body rotation with a peak velocity $\approx 3.2U$ beyond which the velocity drops slightly then increases again to a slightly higher level ($3.4U$) with a flat peak at about $0.5R$. The fully open case still exhibits solid-body rotation within an inner core but no second peak, and the peak velocity has fallen to about $2.7U$ at $r \approx 0.6R$. For $x=25$ mm and beyond, the basic structure of the two sets of profiles remains unchanged, apart from the gradual disappearance of

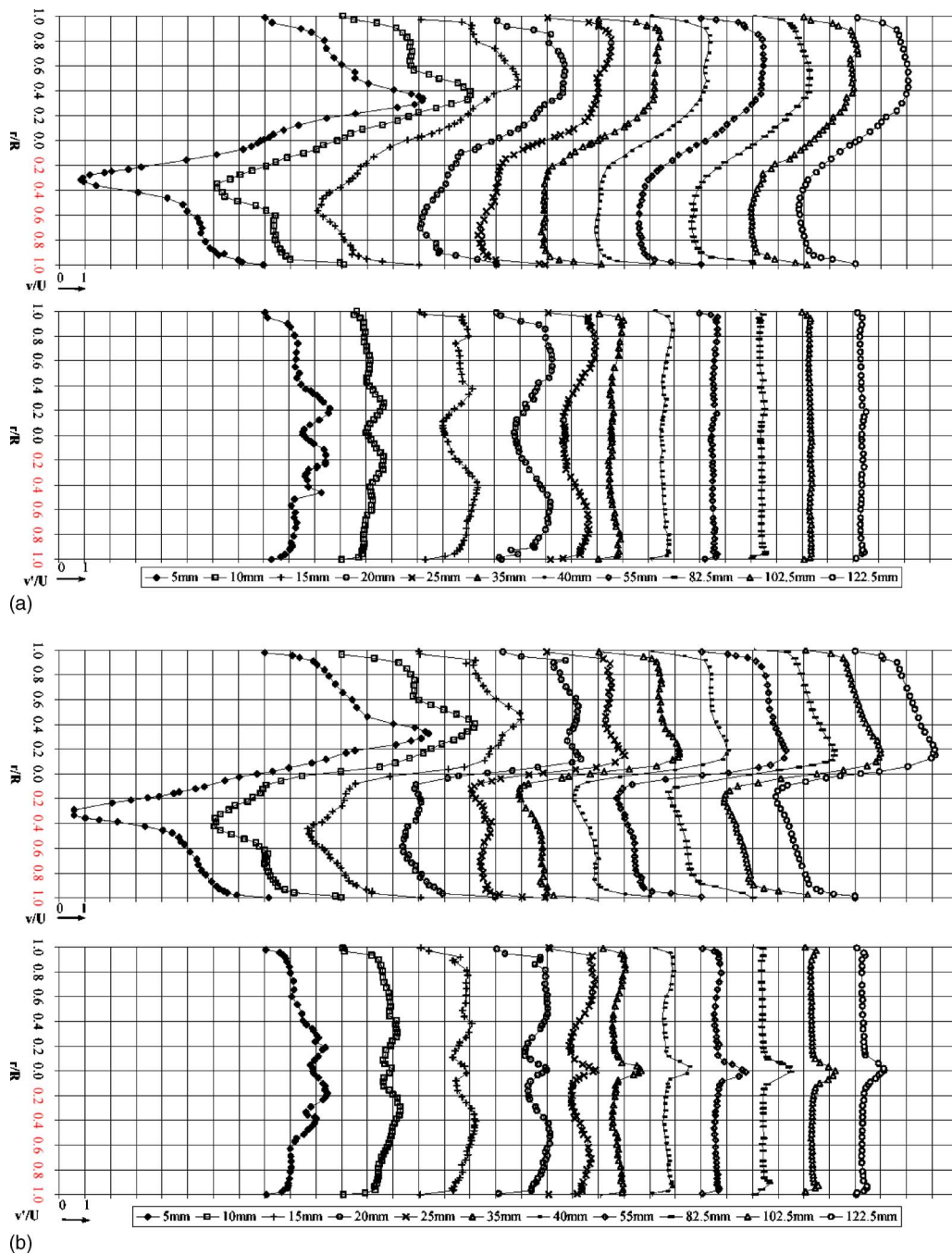


FIG. 8. (a) Radial distributions of mean swirl velocity and swirl-velocity fluctuations for high swirl $S_E=0.6$, fully open outlet. (b) Radial distributions of mean swirl velocity and swirl-velocity fluctuations for high swirl $S_E=0.61$, 25 mm ϕ concentric outlet contraction.

the outer second peak for the contraction case. The boundary-layer regions for the two profiles become almost identical with a peak velocity which drops to about $2U$, and the entire profile for the contraction geometry remains almost unchanged from $x=35$ mm with a well-defined narrow core ($\varphi \approx 0.4R$) and a peak velocity close to $3U$. The more complex profile shapes for both cases in the upstream region ($x/D < 0.4$) are a consequence of the interdependence with the axial-flow field.

As expected from the streamline patterns, the axial-flow profiles shown in Fig. 9 (with spacing corresponding to that used in Fig. 8) reveal complex and different behavior for the

two outlet geometries, although there are still some similarities. That the profiles for the two cases are almost identical until $x=20$ mm seems quite remarkable: as we have just discussed, the swirl profiles reveal qualitative differences as far upstream as we were able to measure, and at $x=20$ mm the swirl profiles for the two cases were very different indeed. Although the streamline patterns were constructed assuming symmetry, close inspection of Fig. 9 reveals a degree of asymmetry away from the axis up to about one tube diameter downstream of the inlet orifice. Further downstream the profiles are essentially symmetrical suggesting that the asymmetry is not associated with the outlet. In fact, asymmetry is a

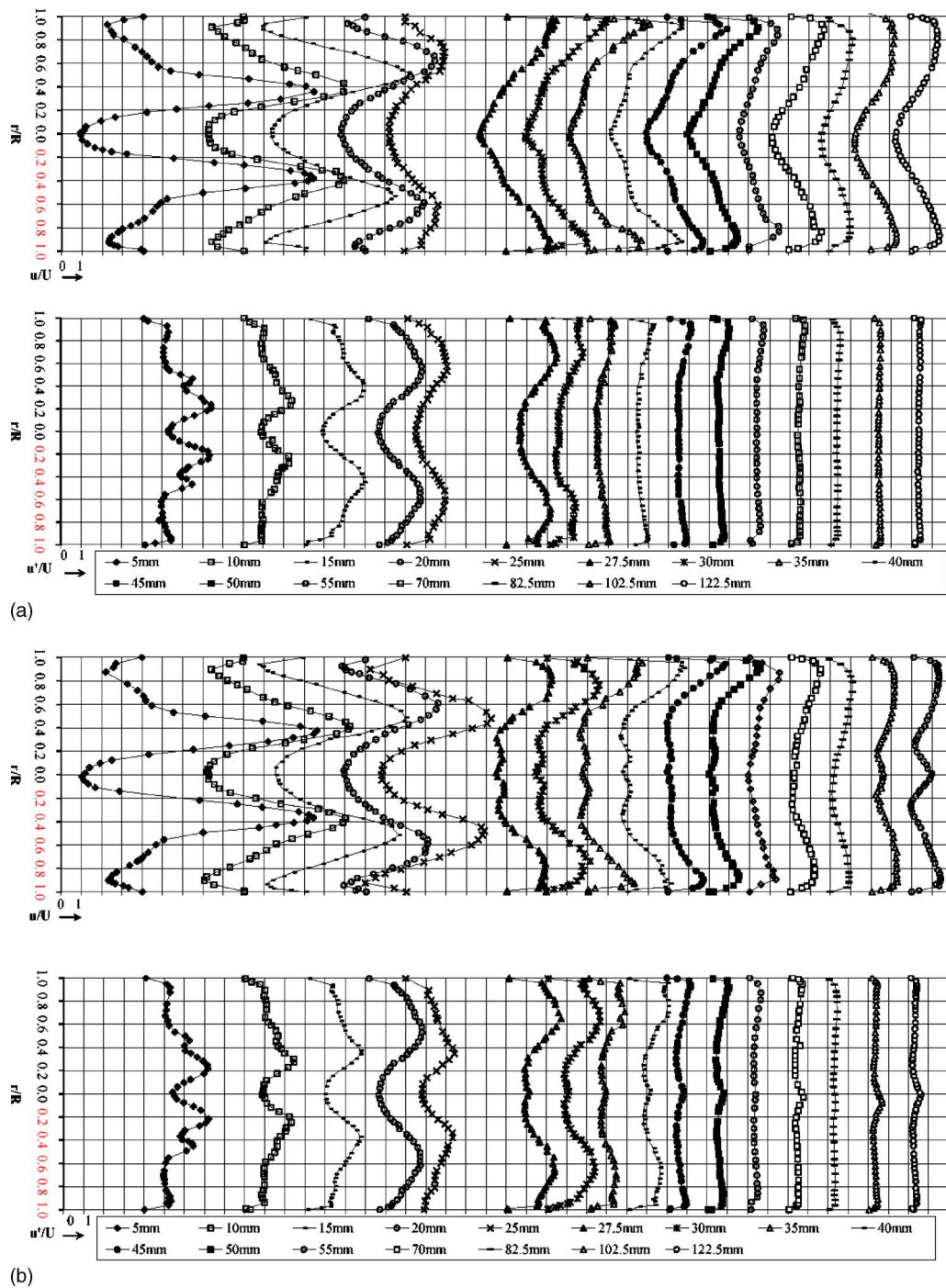


FIG. 9. (a) Radial distributions of mean axial velocity and axial-velocity fluctuations for high swirl $S_E=0.6$, fully open outlet. (b) Radial distributions of mean axial velocity and axial-velocity fluctuations for high swirl $S_E=0.61$, 25 mm ϕ concentric outlet contraction.

well-known phenomenon in nonswirling sudden-expansion flows. The corresponding swirl profiles (Fig. 8) show no significant asymmetry. As was seen from the streamline patterns in Fig. 7(a), for the fully open case there is reverse flow on the centerline throughout the measuring region whereas for the contraction outlet the flow becomes progressively more jet like with downstream distance. Although it could not be measured, it has to be assumed that there is reverse flow upstream of the inlet orifice, possibly even within the swirl generator, which is about three diameters upstream of the orifice. Such behavior has been observed in gas-turbine com-

bustor swirlers (Syed³⁸). The backward flow on the centerline decreases from about $-3U$ at $x=5$ mm to $-U$ at $x=15$ mm while the peak forward velocities decrease rapidly from $8.5U$ at $x=5$ mm to $5U$ at $x=10$ mm but thereafter the decrease is more gradual. Reverse flow, corresponding with the outer recirculation region, is also apparent up to $x=20$ mm for the fully open outlet and $x=25$ mm for the contraction geometry, with a maximum backflow velocity of about $2U$. Up to $x=20$ mm, the locations of the forward velocity peaks coincide almost exactly with those of the peak swirl velocity. By $x=25$ mm, however, the axial-velocity

profile for the fully open outlet has changed significantly whereas the change for the contraction geometry is less marked [although in the latter case it is noticeable that the peak forward velocity occurs at a much larger radius ($r \approx 0.5R$) than for the swirl velocity ($r \approx 0.15R$)]. By the next measuring location, $x=27.5$ mm, however, the correlation between the axial- and swirl-velocity profiles appears to have been partially reestablished, particularly within the vortex core. The axial profiles show that the change from reverse to forward flow occurs at about $x=45$ mm ($x/D=0.81$) for the contraction case, whereas there is reverse flow on the centerline for the fully open geometry even at $x=122.5$ mm. The two profiles at this final measuring station show very clearly the influence of the contraction on the flow within the vortex core: for $r < 0.3R$ the two profiles are qualitatively quite different whereas for $r > 0.3R$ they are almost identical. The complexity of the flow between about $x=27.5$ mm ($x/D=0.5$) and $x=45$ mm illustrates the difficulty encountered in attempting to construct the streamlines shown in Fig. 7(b).

C. High-swirl, $S_E \approx 0.6$, eccentric outlet contraction

The principal reason for performing measurements with an eccentric (or offset) outlet contraction was to investigate the extent to which the core became distorted far upstream, and the swirl and velocity profiles for this outlet showed significant differences to those for the concentric contraction. The profiles of swirl velocity show that with the eccentric outlet contraction the core was indeed distorted and a slightly modified version of the technique adopted by Escudier *et al.*³² was used to locate the vortex axis. The path of the core axis is shown in Fig. 10(a), which shows the core is already offset by about $0.031R$ at the first measuring location ($x = 5$ mm) while the maximum offset is $0.114R$ at $x/D=1.5$. We note that, whereas the flow swirls clockwise around the vortex core, beyond the first measurement position the location of the core axis exhibits an anticlockwise twist until the final measuring location, where the core center is diametrically opposed to the center of the outlet tube. For the most part it can be seen that the swirl profiles in Fig. 11(a), even with the offset caused by the eccentric outlet, bear a striking similarity to the profiles for the concentric contraction which are also included in the figure. One curious difference is the appearance of the inflexion around $r=0$ for the offset case similar to that seen for the fully open exit but which is absent for the concentric contraction. It is also noticeable that the profiles are less symmetrical with the eccentric contraction: peak velocities differ in magnitude and radial location on either side of the vortex axis, the path of which is included in this and subsequent figures where the flow is asymmetrical.

Axial velocity profiles [Fig. 11(b)] were also measured along the diameters which pass through the center of the vortex core. Here again the profiles for the concentric case are included and significant differences are evident, not only in terms of velocity magnitudes and symmetry but also qualitative changes in profile shape. At $x=5$ mm the differences are slight but at $x=10$ mm, the peak velocities (whether for forward flow or backflow) are far higher for the offset case

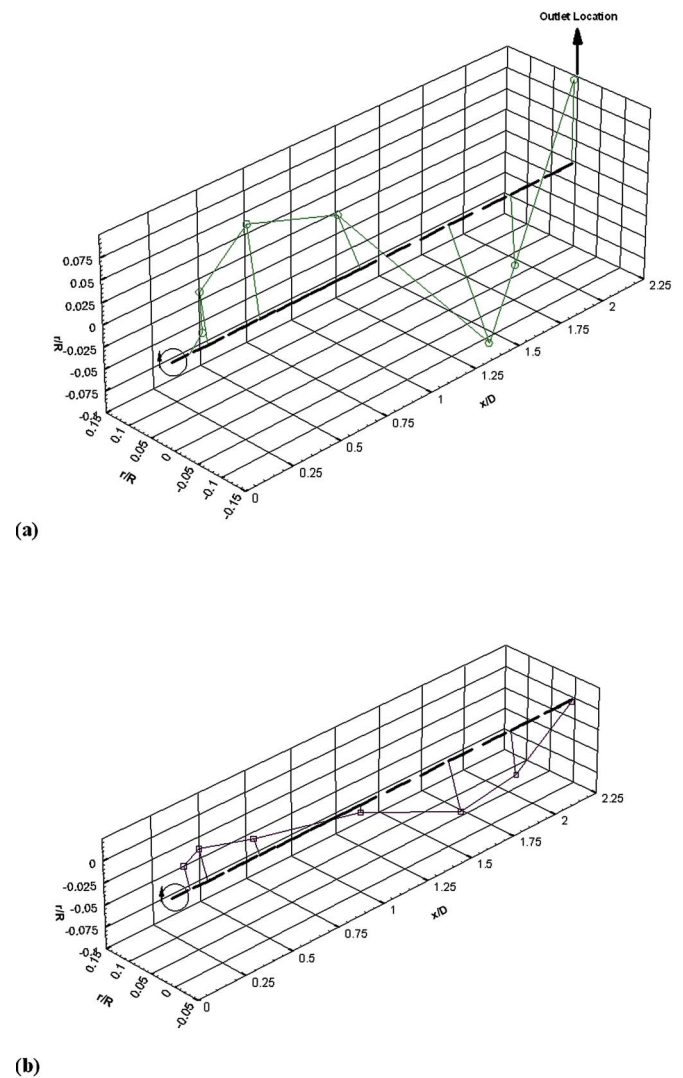


FIG. 10. Path of vortex core for high swirl $S_E \approx 0.6$ for (a) 25 mm ϕ eccentric ($e/D=0.24$) contraction and (b) annular outlet contraction.

than might have been expected from the swirl profiles. At $x=25$ mm the eccentric profile shows a major degree of asymmetry and, in contrast to the previous location, lower peaks, than for the concentric case, and no sign of recirculation near the tube wall. Asymmetry is still present at $x=55$ mm with reverse flow in the core on one side of the vortex center and not the other. Apart from a slight offset for the eccentric geometry (ca. $0.1R$), the corresponding swirl profiles are almost identical. To varying degrees, asymmetry in the axial-velocity profiles is evident throughout the flow. In contrast to the profiles for the concentric outlet, for the eccentric outlet there is significant asymmetry in the core region at all measurement locations. We emphasize, however, that while the core twists about the geometric axis of the vortex tube, it does not precess but remains spatially fixed. In all cases investigated in this study, there were no distinct peaks in the frequency spectra derived from the LDA signals to suggest that the flows were periodic in nature. The three-dimensional character of this flow precluded construction of streamline patterns.

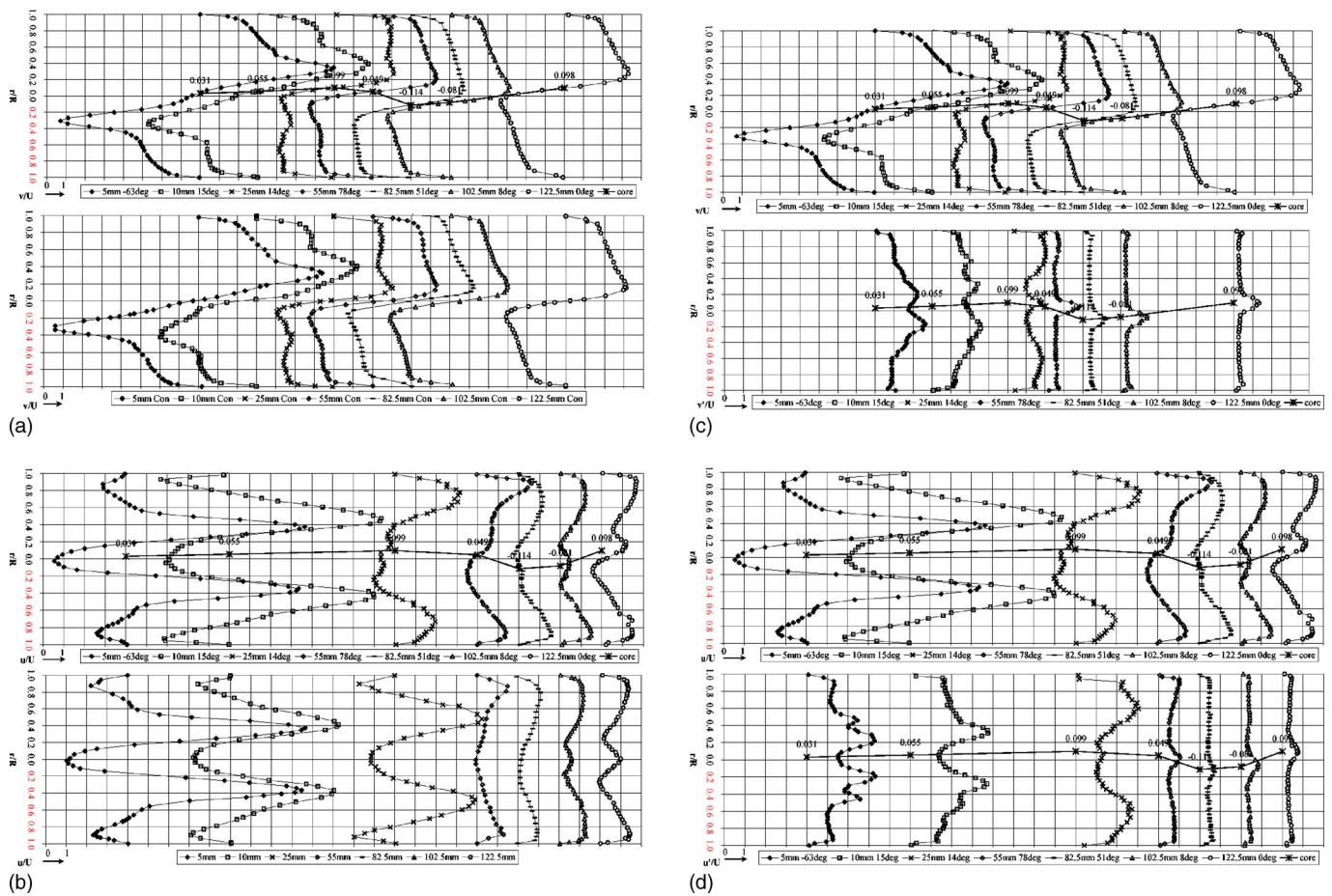


FIG. 11. (a) Radial distributions of mean swirl velocity for high swirl $S_E \approx 0.6$, 25 mm ϕ eccentric contraction and for 25 mm concentric outlet. (b) Radial distributions of mean axial velocity for high swirl $S_E \approx 0.6$, 25 mm ϕ eccentric contraction and for 25 mm concentric outlet. (c) Radial distributions of mean swirl velocity and swirl-velocity fluctuations for high swirl $S_E \approx 0.6$, 25 mm ϕ eccentric outlet contraction. (d) Radial distributions of mean axial velocity and axial-velocity fluctuations for high swirl $S_E \approx 0.6$, 25 mm ϕ eccentric outlet contraction.

D. High-swirl, $S_E \approx 0.6$, concentric annular contraction

The area of the annular gap for this geometry, and hence the contraction ratio, is the same as that for the two previous contraction geometries. With no preferred geometric orientation, the intention was to see how the vortex would adjust to the outlet and, in particular, whether in this case the core might distort and precess giving rise to a periodic flow. As can be seen from the core path in Fig. 10(b), there is some distortion of the core although the maximum departure from the tube axis is slightly less than 50% of that for the eccentric-contraction outlet. However, the core was found to be fixed in space and did not precess. The swirl-velocity profiles have been plotted in Fig. 12(a) and are seen to be very similar to those for the fully open geometry, including the inflexion at the core center for $x=5$ mm although this has disappeared by $x=10$ mm. Overall the annular contraction has a negligible influence on the swirl profiles, with only slight changes in peak values, etc., in contrast to the profiles and core diameter for the previous contraction geometries. The axial-velocity profiles shown in Fig. 12(b) also show greater similarity to those for the fully open case than to those for either of the other two contractions, although there are more significant changes in peak amplitudes than for the swirl profiles: both decrease ($x=5$ and 102.5 mm) and in-

crease ($x=10$, 25, and 82.5 mm). As far upstream as $x=10$ mm the axial-flow profile is quite clearly asymmetric with higher forward velocities to the left of the vortex center and reduced recirculation on the same side. Higher peak velocities on the left-hand side persist until $x=55$ mm but switch to the other side beyond $x=82.5$ mm. These asymmetries are not consistent with the trends shown by the swirl profiles where, for example, the profiles at $x=25$ and 55 mm are practically symmetrical.

E. High-swirl, $S_E \approx 0.6$, double 90° elbow

The differences between the swirl profiles [Fig. 13(a)] for this final case and those for the straight fully open outlet are relatively small, distortion of the vortex core is negligible, and the profiles practically symmetrical. The greatest difference is in the profile closest to the inlet orifice which shows a reduction in peak swirl velocity of about 15%. This profile also shows the inflexion commented on previously but extending to a slightly larger radius than for the straight fully open exit. The axial-velocity profiles shown in Fig. 13(b) are also similar to those for the fully open exit although there are clear differences: the reverse-flow magnitude both on the axis and at the wall at the second and third measuring locations is greater with the double-elbow outlet

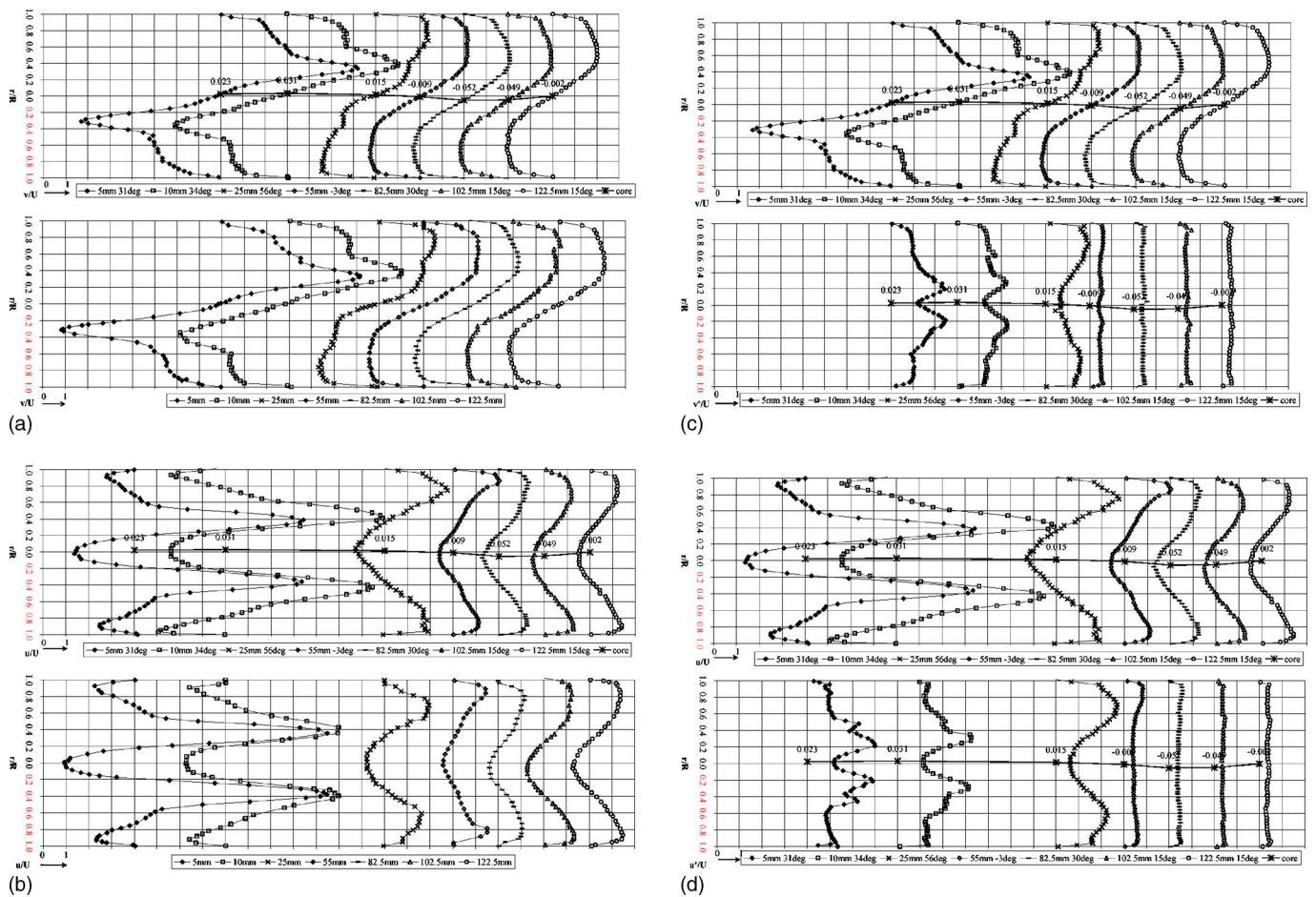


FIG. 12. (a) Radial distributions of mean swirl velocity for high swirl $S_E \approx 0.6$, annular outlet contraction and for fully open outlet. (b) Radial distributions of mean axial velocity for high swirl $S_E \approx 0.6$, annular outlet contraction and for fully open outlet. (c) Radial distributions of mean swirl velocity and swirl-velocity fluctuations for high swirl $S_E \approx 0.6$, annular outlet contraction. (d) Radial distributions of mean axial velocity and axial-velocity fluctuations for high swirl $S_E \approx 0.6$, annular outlet contraction.

and the forward velocities at about $r/R=0.4$ correspondingly higher. Further downstream these trends are reversed.

VI. DISCUSSION OF TURBULENCE-INTENSITY DATA

The turbulence-intensity data for each swirl and outlet condition have been included in Figs. 5, 6, 8, 9, and 11–13. It is possible to identify some links between the trends in the rms fluctuating components of the swirl and axial velocities, v' and u' , and the corresponding distributions of the mean velocities. Rather than discuss each set of data separately, we shall identify these trends, first for v' then for u' , illustrated by reference to appropriate figures. As Zhang and Hugo³⁷ observe regarding their swirling-flow experiments, the axial and swirl flows are characterized by quite different scales. Nevertheless, for simplicity, just as was the case for the mean flow field, we have chosen to normalize the turbulence-intensity values with U , the bulk velocity in the vortex tube. Just as in previous studies, including those of Huang and Yen³⁰ and Zhang and Hugo, very much higher turbulence intensities are observed for intensely swirling flows than for less complex, nonswirling shear flows. Particularly noticeable in many of the v' distributions is a peak on the centerline within the vortex core. Since this central core is a region

of very steep gradients of mean swirl velocity, but negligible shear (solid-body rotation), v' values might also have been expected to be negligible. As was noted in Sec. V, however, the breakdown region is subject to random movement and it is clear that even slight radial movement of the core will lead to large-amplitude fluctuations in the tangential velocity. Huang and Yen suggested that high fluctuations were a consequence of the transformation of momentum from the axial to the tangential direction. As we have also noted, there are no well-defined peaks in the frequency spectra confirming that the fluctuations are essentially random rather than indicative of precession. Centerline peaks are seen in Figs. 5(a) and 5(b) in the upstream region, and further downstream in Figs. 8(b) and 11(c) for the two high-swirl flows with a downstream inner contraction where the core gradient of swirl velocity remains high.

For the most part the axial-velocity fluctuations u' follow the expected pattern of high intensities in regions of high shear which now correspond directly to steep velocity gradients. In Fig. 6(a), for example, at the first upstream location there is a well-defined peak located at around $r/R=0.4$ where the velocity gradient is exceptionally high. Similar peaks are to be found further downstream, initially in the

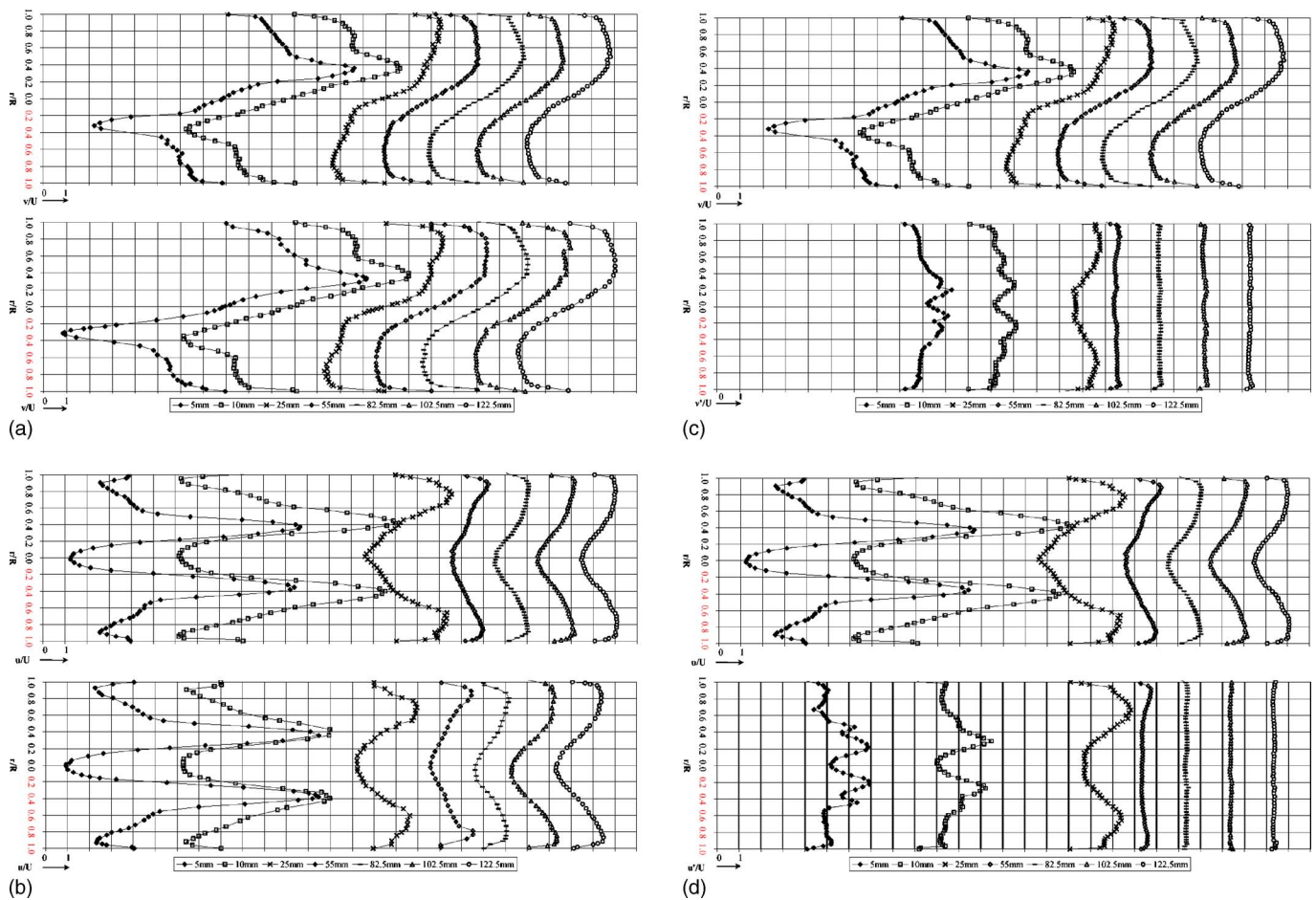


FIG. 13. (a) Radial distributions of mean swirl velocity for high swirl $S_E \approx 0.6$, double 90° elbow outlet, and fully open outlet. (b) Radial distributions of mean axial velocity for high swirl $S_E \approx 0.6$, double 90° elbow outlet, and fully open outlet. (c) Radial distributions of mean swirl velocity and swirl-velocity fluctuations for high swirl $S_E \approx 0.6$, double 90° elbow outlet. (d) Radial distributions of mean axial velocity and axial-velocity fluctuations for high swirl $S_E \approx 0.6$, double 90° elbow outlet.

outer shear layer but also in the inner shear layer surrounding the region of velocity deficit. Although the turbulence at these locations is far from isotropic ($u' > v'$), the argument used earlier for associating centerline peaks in v' with radial movement of the core is supported by the occurrence of similar peaks in u' for the two low-swirl cases, both of which lead to an initially jet-like u profile within the core [Fig. 6(a)] with a sharply defined peak. So far as the high-swirl flows are concerned, the highest turbulence levels in the region immediately downstream of the inlet are observed in the inner shear layers surrounding the central velocity deficit and located at about $r/R \approx 0.2$ [see Figs. 9(a), 9(b), 11(d), 12(d), and 13(d)]. Secondary peaks are seen within the outer ($r/R \approx 0.4$) shear layer in some cases but not others, but generally these peaks seem to disappear with downstream distance at the same time as the highest intensities occur ever closer to the location of the peak mean velocity before decaying to relatively low fairly uniform levels. The relatively high turbulence levels at intermediate locations, we suggest, is a combination of shear-layer production and advection from upstream. In the cases with a central or offset contraction, which lead to a velocity overshoot downstream, there are again peaks in the u' distributions far downstream [Figs. 9(b) and 11(d)], and for the eccentric contraction,

shear associated with the skewing of the mean velocity profile also results in increased turbulence intensity [Fig. 11(d)].

Details of all the LDA measurements reported in this paper can be found at http://www.liv.ac.uk/engdept/research/fluids/vortex_flows/index.htm.

VII. CONCLUSIONS

Detailed LDA measurements of the mean axial and swirl components of velocity have been reported for swirling turbulent pipe flows as they develop downstream of an orifice plate. For the low-swirl case ($S_E \approx 0.3$) the flow is largely unaffected by a central contraction placed six diameters downstream of the inlet orifice, confirming that this flow is supercritical downstream. A closed recirculation bubble (vortex breakdown) occurs centered on the axis just downstream of the inlet. Downstream of this bubble the swirl decays as does the central wake-like deficit in the axial velocity. The high-swirl case ($S_E \approx 0.6$) is much more complex and the flows with and without a concentric central contraction are completely different. In the absence of the contraction there is backflow throughout the vortex core and no closed recirculation region. With the contraction in place, a closed recirculation region is again found centered on the axis but con-

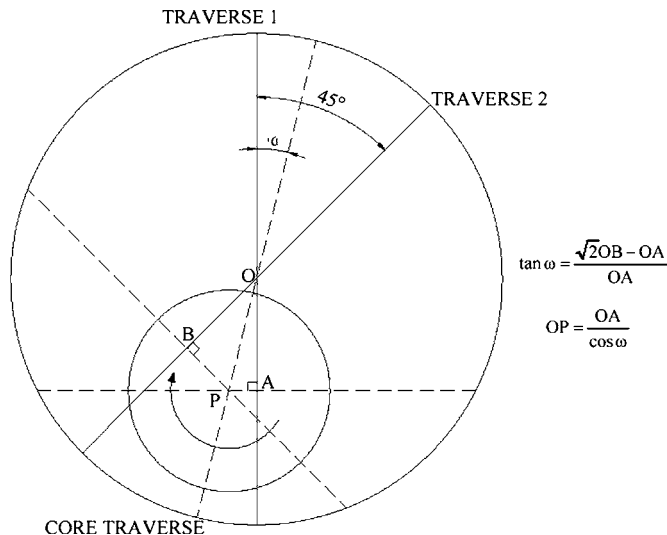


FIG. 14. Method used to determine the position of the vortex core.

siderably distorted when compared with the “simple” elongated smooth shape of the low-swirl vortex breakdown. Downstream of this recirculation region, as the swirl decays, a growing overshoot is found on axis. The strong influence of the outlet contraction confirms that the high-swirl flow is subcritical in the downstream region. In both cases there is an outer annular region of recirculation just downstream of the orifice plate, much as would be the case in the absence of swirl. The flow field is further complicated with an eccentric contraction: both the swirl and axial profiles become asymmetric and the vortex core is distorted along its entire length. An annular contraction also leads to asymmetry and distortion of the core, but to a lesser extent, and the effect of a double-bend outlet is even weaker. Where the vortex core was distorted by the outlet geometry, the measurements show the core was fixed in space with no sign of precession of the core around the tube axis, and spectra derived from the LDA signals confirmed that none of the flows exhibited periodicity. In fact, the mean flow in every case investigated was found to be steady but with high levels of turbulent fluctuation.

ACKNOWLEDGMENT

The research discussed in this paper was supported by EPSRC Grant No. GR/R83613/01.

APPENDIX: PROCEDURE USED TO DETERMINE LOCATION OF VORTEX CORE AXIS

A triangulation procedure, similar to that adopted by Escudier *et al.*,³² was used to establish the radial/angular location of the vortex-core axis for the flows with the eccentric contraction outlet [geometry (c)] and the annular contraction outlet [geometry (d)]. The underlying assumption is that the vortex core of these asymmetric flows can be approximated by an axisymmetric flow centered on an offset axis. To find the location of this axis at a given x location, a first radial profile of the swirl velocity $v(r)$ was obtained. The vortex tube was then rotated through 45° and a second swirl-

velocity profile $v(r)$ obtained. The distances from the tube centerline of the location of zero velocity in each case were then determined, and from these values the triangulation procedure shown in Fig. 14 was used to determine the location of the center of the vortex core in terms of radial distance from the tube centerline and angle from the zero position. It is assumed that for the initial traverse along the $\theta=0^\circ$ diameter, the swirl velocity is zero at point A and for the traverse along the $\theta=45^\circ$ the corresponding location is point B. If it is assumed that the core is axisymmetric, the construction to find the axis location P follows. It should be noted that the distances OA, OB, and OP are all exaggerated in Fig. 14. Once the location of the axis was established, the vortex tube was rotated to this angular position and the swirl and axial-velocity profiles measured along the diameter passing through P. The procedure was repeated for each individual x location.

- ¹S. Hogg and M. A. Leschziner, “Computation of highly swirled confined flow with a Reynolds stress turbulence model,” *AIAA J.* **27**, 57 (1989).
- ²H. B. Squire, “Analysis of the vortex breakdown phenomenon,” in *Miszellen der Angewandten Mechanik*, edited by M. Schaefer (Akademie Verlag, Berlin, 1962), p. 306.
- ³T. B. Benjamin, “Theory of the vortex breakdown phenomenon,” *J. Fluid Mech.* **14**, 593 (1962).
- ⁴T. B. Benjamin, “Significance of the vortex breakdown phenomenon,” *J. Basic Eng.* **87**, 518 (1965).
- ⁵T. B. Benjamin, “Some developments in the theory of vortex breakdown,” *J. Fluid Mech.* **28**, 65 (1967).
- ⁶M. P. Escudier, “Vortex breakdown: Observations and explanations,” *Prog. Aerosp. Sci.* **25**, 189 (1988).
- ⁷J. C. Chen and C. A. Lin, “Computations of strongly swirling flows with second-moment closures,” *Int. J. Numer. Methods Fluids* **30**, 493 (1999).
- ⁸X. Yang and H. Ma, “Cubic eddy-viscosity turbulence models for strongly swirling confined flows with variable density,” *Int. J. Numer. Methods Fluids* **45**, 985 (2004).
- ⁹X. Yang and H. Ma, “Computation of strongly swirling flows with cubic eddy-viscosity turbulence models,” *Int. J. Numer. Methods Fluids* **33**, 1355 (2003).
- ¹⁰S. Jakirlic, R. Jester-Zuerker, and C. Tropea, “Joint effects of geometry confinement and swirling inflow on turbulent mixing in model combustors: a second-moment closure study,” *Prog. Comput. Fluid Dyn.* **4**, 198 (2004).
- ¹¹R. E. Spall and T. B. Gatski, “Numerical calculations of three-dimensional turbulent vortex breakdown,” *Int. J. Numer. Methods Fluids* **20**, 307 (1995).
- ¹²M. H. Aksel and M. T. Kaya, “A numerical simulation of the axisymmetric vortex breakdown in a tube,” *Appl. Math. Model.* **16**, 414 (1992).
- ¹³C. F. Stein, “Toward a vortex breakdown condition for swirling annular jets,” *ASME Trans. J. Fluids Eng.* **121**, 102 (1999).
- ¹⁴W.-W. Kim, S. Menon, and H. C. Mongia, “Large-eddy simulation of a gas turbine combustor flow,” *Combust. Sci. Technol.* **143**, 25 (1999).
- ¹⁵D. L. Darmofal, “Comparisons of experimental and numerical results for axisymmetric vortex breakdown in pipes,” *Comput. Fluids* **25**, 353 (1996).
- ¹⁶J. L. Xia, B. L. Smith, A. C. Benim, J. Schmidli, and G. Yadigaroglu, “Effect of inlet and outlet boundary conditions on swirling flows,” *Comput. Fluids* **26**, 811 (1997).
- ¹⁷D. I. Young, C. B. Liao, and R. J. Sheen, “Computations of recirculation zones of a confined annular swirling flow,” *Int. J. Numer. Methods Fluids* **29**, 791 (1999).
- ¹⁸M. I. Yaras and A. D. Grosvenor, “Evaluation of one- and two-equation low-Re turbulence models. Part I—Axisymmetric separating and swirling flows,” *Int. J. Numer. Methods Fluids* **42**, 1293 (2003).
- ¹⁹M. A. Herrada and R. Fernandez-Feria, “On the development of three-dimensional vortex breakdown in cylindrical regions,” *Phys. Fluids* **18**, 084105 (2006).

- ²⁰H. Altgeld, W. P. Jones, and J. Wilhelmi, "Velocity measurements in a confined swirl driven recirculating flow," *Exp. Fluids* **1**, 73 (1983).
- ²¹R. M. C. So, S. A. Ahmed, and H. C. Mongia, "An experimental investigation of gas jets in confined swirling air flow," NASA Report No. CR3832, 1984.
- ²²M. P. Escudier and J. J. Keller, "Recirculation in swirling flows: a manifestation of vortex breakdown," *AIAA J.* **23**, 111 (1985).
- ²³S. A. Ahmed and A. S. Nejad, "Velocity measurements in a research combustor. Part 1: Isothermal swirling flow," *Exp. Therm. Fluid Sci.* **5**, 162 (1992).
- ²⁴K. Doebbeling, B. Lenze, and W. Leuckel, "Four-sensor hot-wire probe measurements of the isothermal flow in a model combustion chamber at different levels of swirl," *Exp. Therm. Fluid Sci.* **5**, 381 (1992).
- ²⁵L. Khezzar, "Velocity measurements in the near field of a radial swirler," *Exp. Therm. Fluid Sci.* **16**, 230 (1998).
- ²⁶R. F. Huang and F. C. Tsai, "Observations of swirling flows behind circular disks," *AIAA J.* **39**, 1106 (2001).
- ²⁷R. F. Huang and F. C. Tsai, "Flow field characteristics of swirling double concentric jets," *Exp. Therm. Fluid Sci.* **25**, 151 (2001).
- ²⁸R. F. Huang and F. C. Tsai, "Flow and mixing characteristics of swirling wakes in blockage-effect regime," *J. Wind. Eng. Ind. Aerodyn.* **92**, 199 (2004).
- ²⁹F. Schmitt, B. K. Hazariki, and C. Hirsch, "LDV measurements of the flow field in the nozzle region of a confined double annular burner," *ASME Trans. J. Fluids Eng.* **123**, 228 (2001).
- ³⁰R. F. Huang and S. C. Yen, "Axisymmetric swirling vertical wakes modulated by a control disk," *AIAA J.* **41**, 888 (2003).
- ³¹Y. M. Al-Abdeli and A. R. Masri, "Precession and recirculation in turbulent swirling isothermal jets," *Combust. Sci. Technol.* **176**, 645 (2004).
- ³²M. P. Escudier, J. Bornstein, and N. Zehnder, "Observations and LDA measurements of confined turbulent vortex flow," *J. Fluid Mech.* **98**, 490 (1980).
- ³³M. P. Escudier, "Vortex breakdown and the criterion for its occurrence," in *Intense Atmospheric Vortices*, edited by L. Bengtsson and J. Lighthill (Springer-Verlag, Berlin, 1982), p. 247.
- ³⁴B. Pak, Y. I. Cho, and S. U. S. Choi, "Separation and reattachment of non-Newtonian fluid flows in a sudden expansion pipe," *J. Non-Newtonian Fluid Mech.* **37**, 175 (1990).
- ³⁵M. A. Herrada, M. Pérez-Saborid, and A. Barrero, "Nonparallel local spatial stability analysis of pipe-entrance swirling flows," *Phys. Fluids* **16**, 2147 (2004).
- ³⁶A. K. Gupta, D. G. Lilley, and N. Syred, *Swirl Flows* (Abacus, Tunbridge Wells, 1984).
- ³⁷Z. Zhang and R. J. Hugo, "Stereo particle image velocimetry applied to a vortex pipe flow," *Exp. Fluids* **40**, 333 (2006).
- ³⁸K. Syed, Siemens Gas Turbines Ltd. (private communication).